ANALYSIS
https://doi.org/10.1038/s41893-020-00643-w

nature sustainability

Climate change extremes and photovoltaic power output

Sarah Feron[1,2], Raúl R. Cordero[1]✉, Alessandro Damiani[3] and Robert B. Jackson[2,4]

Sustainable development requires climate change mitigation and thereby a fast energy transition to renewables. However, climate change may affect renewable power outputs by enhancing the weather variability and making extreme conditions more frequent. High temperature or clouds, for example, can lead to poorer photovoltaic (PV) power outputs. Here, we assess global changes in the frequency of warm and cloudy conditions that lead to very low PV power outputs. Using simulations from global climate models (RCP4.5 and RCP8.5), we show that summer days with very low PV power outputs are expected to double in the Arabian Peninsula by mid-century but could be reduced by half in southern Europe over the same period, even under a moderate-emission scenario. Changes for winter, either enhancing or mitigating the PV power intermittency, are projected to be less striking, at least in low- and mid-latitude regions. Our results present valuable information for energy planners to compensate for the effects of future weather variability.

Renewables are considered a key tool for making progress towards United Nations Sustainable Development Goal 7, which entails universal access to affordable, reliable and modern energy[1]. Renewable energies can also help reduce global emissions and hence mitigate climate change[2]. Decentralized renewable energy projects, based on solar photovoltaic (PV) systems, also have the potential to contribute to climate change adaptation, climate resilience, energy security and social justice[1]. However, the sensitivity of renewables to future weather variability is a source of uncertainty that may complicate energy planning and compromise investments in the energy sector.

Although PV power capacity is expected to dominate growth in the renewable capacity in the foreseeable future[2], PV power outputs change with climate. For example, changes in the frequency of warm, cloudy weather can substantially alter PV energy yields. PV energy yields depend on the downwelling shortwave (SW) irradiance (I), which is in turn modulated by aerosols[3–7] and by clouds[8,9]. PV outputs are also affected by air temperature (T) (with cooler conditions generally improving PV cell performance and hotter conditions reducing it[10,11]) and by surface wind speed (v) (air flow typically cools the PV module[12]).

While climate change is likely to increase future energy demand[13], it can also complicate projections of PV energy yields by changing I, v and T. Several studies have addressed this issue using global climate models (GCMs)[14–16] or regional climate models (RCMs)[17–19]. Here, we focus on the effects of unusual weather and climate extremes on PV power outputs. For example, the concurrence of high temperatures and overcast conditions during one or more consecutive days can reduce PV power outputs. Changes in the frequency of these extremes can either reinforce or mitigate PV power intermittency, with implications for grid planning and operations.

By applying a widely used approach[20,21] for assessing changes in the probability of occurrence of extreme events, we have assessed the progression and expected changes in the number of days with very low PV power outputs (defined according to the 10th percentile). Three metrics were used: the share of days with very low PV power outputs (PV10), the number of events of very low power outputs per season (PV10N) and the length in days of the longest event during a season (PV10D); we defined an event as a period of at least three consecutive days of very low power outputs. Additional comparisons involved computing the share of days with very high PV power outputs (PV90; defined according to the 90th percentile).

As a proxy of the PV power output, we used the PV potential (PV_{POT}), which is defined as the fraction of the power output generated under standard conditions that a PV module may exhibit in the field[22–26]. We computed daily PV_{POT} values using daily estimates of I, v and T rendered by seven GCMs from the Coupled Model Intercomparison Project 5 (CMIP5)[27] (see Supplementary Table 1 for the details). The daily PV_{POT} values ranged from relatively high values (often associated with cloudless conditions) to relatively low values (associated with warm and/or cloudy weather).

We considered very low (or very high) daily PV power outputs to be those falling below the 10th (or above the 90th) percentile of the probability density function (PDF) of the daily PV_{POT} anomalies (the departure of the daily PV_{POT} value from the daily base climatology). GCM-based estimates of the daily PV_{POT} data computed over a base period of 30 years (1961–1990) allowed us to define a daily base climatology, from which the daily PV_{POT} anomalies were calculated.

Results

Climate change is expected to change average PV power outputs to only a minor to moderate extent under the Representative Concentration Pathway 4.5 (RCP4.5) scenario (that is, the RCP that stabilizes radiative forcing at 4.5 W m^{-2} in the year 2100)[28]. As shown in Fig. 1a, moderate changes (either positive or negative) are expected by mid-century in summer PV_{POT} estimates in parts of the Arabian Peninsula (−4%) and central Europe (+5%). The changes in PV_{POT} are less pronounced in other regions such as the Atacama Desert (+3%), southeastern Australia (−2%), eastern China and southeastern Asia (+2%), northwestern Africa (−2%),

[1]Universidad de Santiago de Chile, Santiago, Chile. [2]Department of Earth System Science, Stanford University, Stanford, CA, USA. [3]Center for Environmental Remote Sensing, Chiba University, Chiba, Japan. [4]Woods Institute for the Environment and Precourt Institute for Energy, Stanford University, Stanford, CA, USA. ✉e-mail: raul.cordero@usach.cl

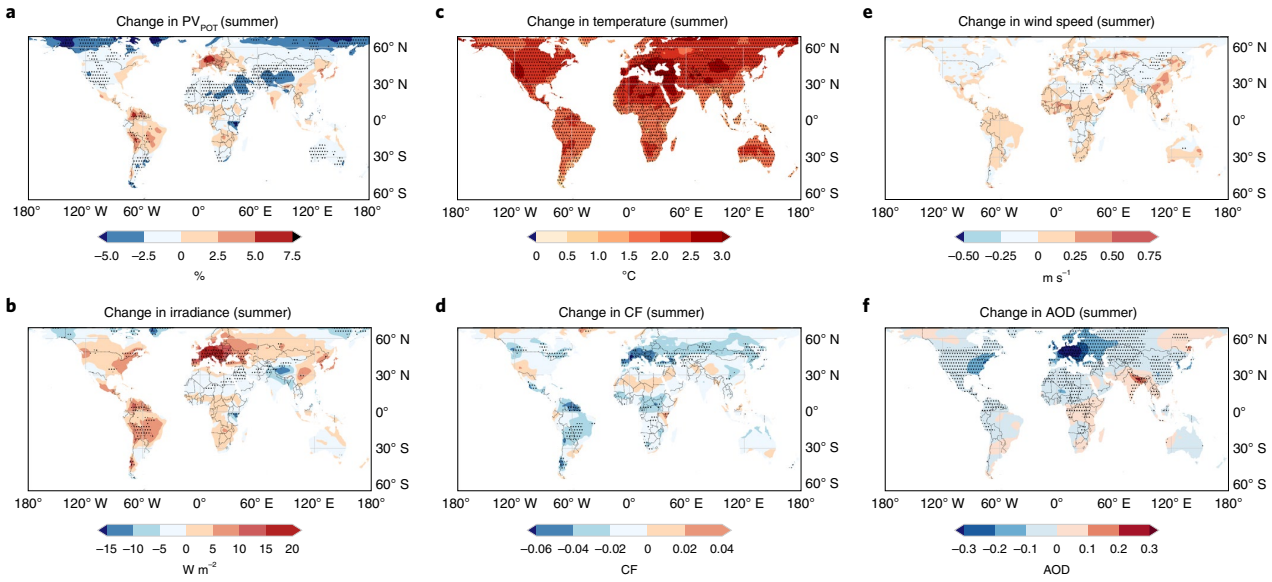

Fig. 1 | Future changes in solar potential for summer are on average moderate worldwide. a–f, Changes from 1961–1990 to 2036–2065 (RCP4.5) in the multimodel mean (MMM) of GCM-based summer estimates of PV_{POT} estimates (**a**), downwelling SW irradiance (**b**), surface ambient temperature (**c**), CF (**d**), surface wind speed (**e**) and AOD (**f**). The plots were made by assembling December–February (DJF) data for the Southern Hemisphere and June–August (JJA) data for the Northern Hemisphere. Stippling indicates regions where the detected changes are considered to be significant. The plots were generated using Python's Matplotlib library[43].

the southwestern United States (−2%), the northeastern United States (+2%) and central Asia (−3%).

The PV_{POT} changes for summer are mostly driven by changes in SW irradiance (Fig. 1b), which are, in turn, influenced by clouds and aerosols. As warm conditions affect solar cell performance, the PV_{POT} estimates in Fig. 1a are also influenced by the expected rise in air temperature (Fig. 1c). Changes in cloud fraction (CF) (Fig. 1d), wind speed (Fig. 1e) and aerosol optical depth (AOD) (Fig. 1f) may either reinforce the effect of increasing temperatures or offset (and even outpace) this effect. The latter is the case for central Europe, where the PV_{POT} is expected to increase (+5%) by mid-century, mostly attributable to the expected drop in both aerosols[7,16] and cloudiness[29,30].

In agreement with prior efforts[18,19,22], Fig. 1a also shows that moderate changes in the PV solar potential (less than ±3%) are projected for most of Africa, except for eastern Africa (around Tanzania), where slightly greater reductions in summer PV_{POT} are projected. The PV_{POT} changes expected for the Sahel region (Fig. 1a) are not considered to be significant due to the uncertainty associated with the cloud estimates in that region[31]. Nevertheless, note that comparisons with prior efforts need to be taken with caution, given the different models used and the different reference period adopted.

As shown in Fig. 2a, PV_{POT} changes for winter are expected to occur nearly in the same direction as those expected for summer. However, the magnitude of the changes differs in some regions. For example, because the drop in clouds (Fig. 2d) and aerosols (Fig. 2f) is projected to be less substantial in winter than in summer for central Europe, the corresponding PV_{POT} increases are projected to be less pronounced in winter than in summer. In contrast, and consistent with previous efforts[23], PV_{POT} estimates in high-latitude regions in the Northern Hemisphere (Fig. 2a) are expected to drop more intensely in winter than in summer due to a sharp increase in cloudiness expected in these regions (Fig. 2d); indeed, CMIP5 models project an increase in the CF over the Arctic Ocean and high-latitude land regions during this century, especially in the months and regions of greatest Arctic sea-ice loss[32]. Figures 1a and 2a show that changes in the average PV_{POT} estimates expected by mid-century under the RCP4.5 scenario range from minor to moderate around the world. However, as shown below, these relatively modest changes mask important changes in the number of days with very low PV power outputs.

Summer days with very low PV power outputs (PV10) are expected to drop by about 50% in southern Europe by mid-century but could increase by more than 100% in the Arabian Peninsula over the same period, even under a moderate-emission scenario (RCP4.5). As shown in Fig. 3a, changes in PV10 estimates are also important in other regions of high solar PV energy potential; the share of very low PV output days in the southwestern United States is expected to increase by about 30% under the RCP4.5 scenario, while PV10 estimates are expected to fall by about 30% in southern Germany under the same scenario. The changes are less pronounced (lower than ±20%) in southern Africa, southeastern Australia, northwestern Africa, eastern China, southeastern Asia and the Atacama Desert.

In mid-latitude regions, changes in PV10 estimates are projected to be less pronounced in winter than in summer. The opposite is true for high-latitude regions. For example, PV10 estimates are expected to increase in the Arabian Peninsula by about 40% in winter (Fig. 3b) but could rise by more than 100% in summer (Fig. 3a). However, the increase in cloudiness projected in winter in high-latitude regions (Fig. 2d) is expected to lead to increments of more than +50% in PV10 estimates by mid-century in the Northern Hemisphere (Fig. 3b).

The changes in PV10N (Fig. 3c,d) and PV10D (Fig. 3e,f) are also considerably greater in summer than in winter, especially in low-latitude regions. As noted above, an event was defined as a period of three consecutive days with very low power outputs. While increases in PV10N (as well as in the number of days with very low PV power outputs) may boost PV power intermittency and affect the network stability[33], increments in the longest event during

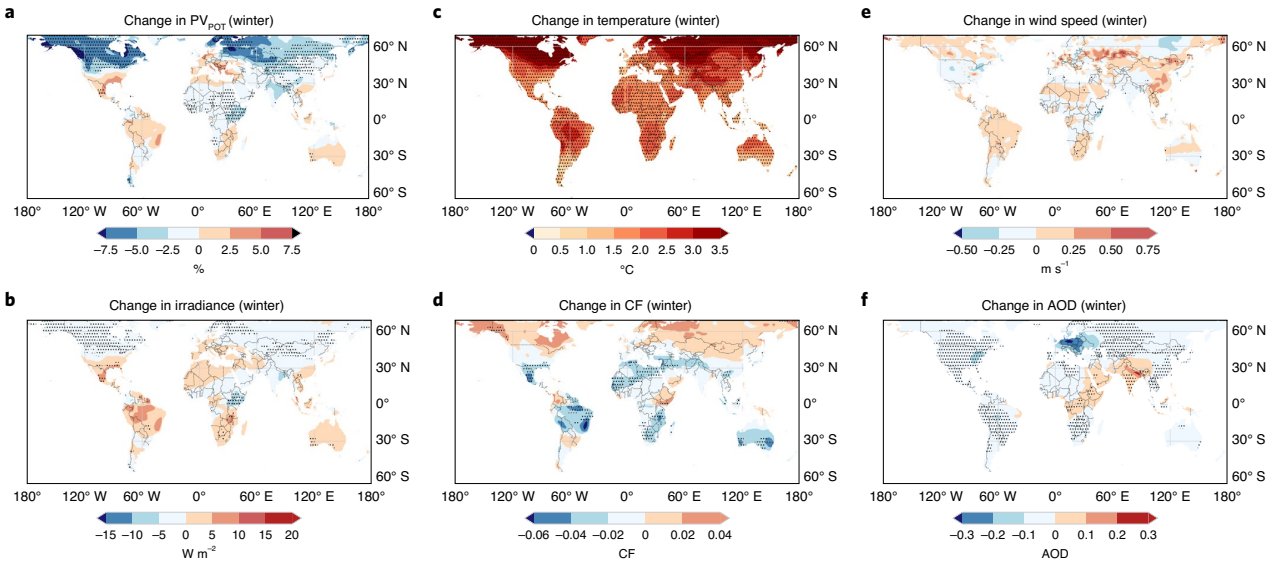

Fig. 2 | Future changes in solar potential for winter are only relevant at high latitudes. a–f, Changes from 1961–1990 to 2036–2065 (RCP4.5) in the MMM of GCM-based winter estimates of PV_{POT} estimates (**a**), downwelling SW irradiance (**b**), surface ambient temperature (**c**), CF (**d**), surface wind speed (**e**) and AOD (**f**). The plots were made by assembling JJA data for the Southern Hemisphere and DJF data for the Northern Hemisphere. Stippling indicates regions where the detected changes are considered to be significant. The plots were generated using Python's Matplotlib library[43].

a season may also increase the need for enhanced energy storages and backup power[34]. As shown in Fig. 3c–f, the Arabian Peninsula and northeastern Africa may undergo more than two events every summer by mid-century (currently they have typically one per summer), and the longest of these events may last up to eight days (currently the longest event in summer typically lasts less than five days). Changes in PV10N and PV10D values are expected to be less striking for the rest of the world. However, the southwestern United States, southeastern Asia and northern India may undergo one or two events every summer by mid-century (currently they typically have one per summer), and the longest of these events may last up to four to six days (currently the longest event in summer typically lasts about three to four days). Changes for winter in low and mid-latitude regions exhibit similar regional features, but they are projected to be less striking. As a reference, Supplementary Fig. 1 (summer) and Supplementary Fig. 2 (winter) show the PV10N and PV10D values computed over the base period (1961–1990) and over mid-century (2036–2065).

Note that although the changes shown in Fig. 3 are relative to a base period (1961–1990), changing the reference period to 1971–2000, for example, does not change the main trends. Supplementary Fig. 3 shows the same results shown in Fig. 3 but computed by using 1971–2000 as the base period. Unsurprisingly, the results in Supplementary Fig. 3 exhibit the same regional features as those in Fig. 3. However, the changes in the PV10 metrics from the base period to mid-century in Supplementary Fig. 3 are slightly smaller than those shown in Fig. 3; this was expected because the base period in Supplementary Fig. 3 (1971–2000) is closer to mid-century than the base period in Fig. 3 (1961–1990).

Changes in the PV10 estimates (Fig. 3a,b) are consistent with the PV_{POT} changes projected by mid-century (Figs. 1a and 2a); important changes in PV10 estimates are associated with important changes in PV_{POT} estimates. This is the case for southern Europe, where a decrease of about 50% in the frequency of very low PV output days (Fig. 3a) is expected to contribute to an increase in the PV_{POT} of about 5% by mid-century (Fig. 1a). It also occurs in the Arabian Peninsula, where a sharp increase of more than 100% in PV10 (Fig. 3a) is expected to contribute to a drop in the PV_{POT} of about 4% by mid-century (Fig. 1a).

Changes in the frequency of very low PV output days (Fig. 3a,b) are also consistent with changes in PV90. The changes in PV90 estimates, both in summer (Supplementary Fig. 4a) and in winter (Supplementary Fig. 4b), generally mirror the changes in PV10 shown in Fig. 3a,b. For example, important increases in the frequency of very low PV output days, such as those expected by mid-century in the Arabian Peninsula (Fig. 3a), are associated with substantial decreases in the frequency of very high PV output days (Supplementary Fig. 4a). However, there are cases in which moderate changes in PV10 correspond to substantial changes in PV90. For example, moderate increases in PV10 estimates expected by mid-century in northern India (Fig. 3b) are associated with sharp drops in PV90 estimates that can exceed 50% (Supplementary Fig. 4b). These nonlinearities result from the skewed PDFs of the daily PV_{POT} anomalies (Supplementary Fig. 5), as the long left-hand tails of these PDFs can make PV10 less sensitive to changes in the dispersion of PV power outputs than PV90. The steep drop in PV90 estimates expected by mid-century in northern India (Supplementary Fig. 4b) is strongly influenced by the considerable increase in the aerosol load projected in the region[35].

Although changes in PV10 estimates (Fig. 3a,b) depend on several factors, the SW irradiance has a dominant effect. Figure 4 shows the change in PV10 estimates attributable to changes in SW irradiance (Fig. 4a,b), temperature (Fig. 4c,d) and wind (Fig. 4e,f). As shown in Fig. 4a,b, most of the changes in the frequency of very low PV output days result from changes in the SW irradiance (which are in turn driven by clouds and aerosols). For example, in good agreement with prior efforts[7,8], we found that both cloudiness and aerosols are expected to decrease in southern Europe in summer (Fig. 1d,f), leading in turn to the sharp drop in the very low PV output days expected by mid-century in this region (Fig. 3a).

Changes in winter clouds (Fig. 2d) are the main driver of the severe PV10 increases expected in high-latitude regions in the Northern Hemisphere (Fig. 3b). Clouds are also involved in the changes expected in northeastern Africa and the Arabian Peninsula.

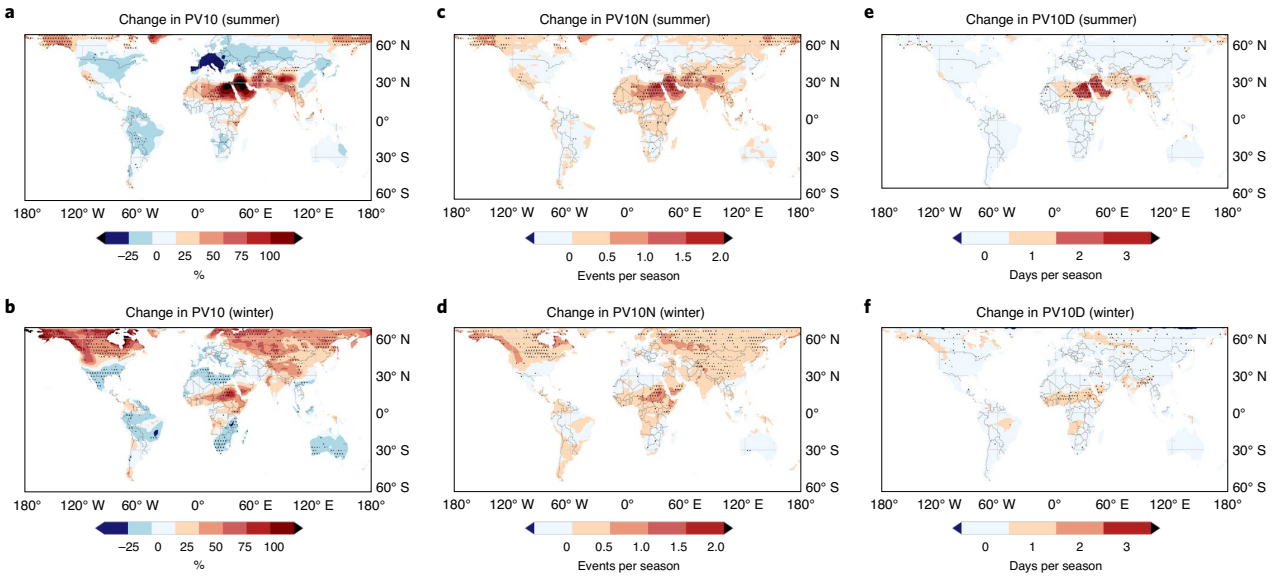

Fig. 3 | Changes in PV power intermittency for summer are expected to be stronger in Europe and the Arabian Peninsula. a–f, Changes from 1961–1990 to 2036–2065 (RCP4.5) in PV10 (**a**,**b**), PV10N (**c**,**d**) and PV10D (**e**,**f**). The plots corresponding to summer (**a**,**c**,**e**) were made by assembling DJF data for the Southern Hemisphere and JJA data for the Northern Hemisphere, while the plots corresponding to winter (**b**,**d**,**f**) were made by assembling JJA data for the Southern Hemisphere and DJF data for the Northern Hemisphere. Stippling indicates regions where the detected changes are considered to be significant. The plots were generated using Python's Matplotlib library[43].

Although minor changes in the mean summer cloudiness are expected in these regions by mid-century (Fig. 1d), an increase of about 5% is projected by mid-century in the cloudiness variability (characterized by the s.d. of the daily CF) (Supplementary Fig. 6). This enhanced cloudiness variability explains most of the summer PV10 changes shown in Fig. 4a in the Arabian Peninsula.

The influence of temperature becomes important in extremely warm regions. For example, increases in extreme heat account for a great fraction of the changes expected in the PV10 estimates by mid-century in northeastern Africa and the Arabian Peninsula (Fig. 4c). In these extremely warm regions[36], heat waves are expected to increase by four to five times by mid-century under the RCP4.5 scenario[37]. The increases in episodic extreme heat considerably reinforce the effect of the enhanced cloudiness variability, which in turn leads to nearly a doubling in summer PV10 estimates in northeastern Africa and in the Arabian Peninsula under the RCP4.5 scenario (Fig. 3a). Supplementary Fig. 7 confirms that the sharpest drops in the summer PV power outputs expected by mid-century (in northeastern Africa and the Arabian Peninsula) result from the more frequent concurrence of high temperatures and clouds. The results shown in Supplementary Fig. 7 were computed by applying a widely used approach[38] for assessing changes in the probability of occurrence of concurrent extremes (Methods). Compared with the influence of clouds and temperature, the influence of wind speed changes on the PV10 estimates is negligible (Fig. 4e,f).

As expected, the changes tend to be more pronounced under a high-emission scenario. Supplementary Figs. 8 and 9 depict the changes from 1961–1990 to 2036–2065 (RCP8.5) in PV_{POT} estimates, air temperature, wind speed, SW irradiance, CF, AOD and PV10 estimates (summer and winter). These figures show that changes under the RCP8.5 scenario are more striking but are basically consistent with those projected under the RCP4.5 scenario.

Discussion

The mitigation of fossil fuel use and climate change requires a fast energy transition, within which solar PV power is expected to play a key role. However, a sustainable energy transition requires reliable planning to compensate for potential changes in climate regimes throughout the entire lifespan of the PV systems. Future climate may enhance the weather variability, increase the renewable power intermittency and thereby increase the need for energy storage and grid stabilization services. Understanding the response of the PV power outputs to changing climate regimes is crucial for an energy transition and in turn for sustainable development.

Prior efforts[14–19] have addressed the influence of a changing climate on future PV power outputs, finding that climate change is expected to lead to relatively modest changes in average PV energy yields. However, these prior efforts have not generally accounted for the influence on PV power outputs of the enhanced weather variability (associated with the future climate in vast parts of the world). Although our results confirm that the average PV energy yields are expected to change to only a minor to moderate extent (under the RCP4.5 scenario), they highlight the fact that these relatively modest changes mask substantial shifts in the number of days with very low PV power outputs.

Future climate will change the frequency of weather conditions that lead to very low PV power outputs. These changes are a source of uncertainty that may complicate energy planning and compromise investments in the energy sector in the near future. While a drop in cloudiness, for example, may improve the network reliability, an increase in warm or cloudy conditions may boost very low PV power outputs during short periods of time, affecting the network stability.

We have shown that substantial increases in the frequency of weather conditions that lead to very low PV power outputs are expected in large regions of the world by mid-century. Generally driven by more clouds, conditions leading to poorer PV power outputs can be reinforced in some low-latitude regions by increasingly extreme temperatures. This is case in the Arabian Peninsula and in northeastern Africa, where, due to the more frequent concurrence of high temperatures and clouds, summer days with very low PV power outputs are expected to double by mid-century. However, we also show that in some other regions, the frequency of conditions

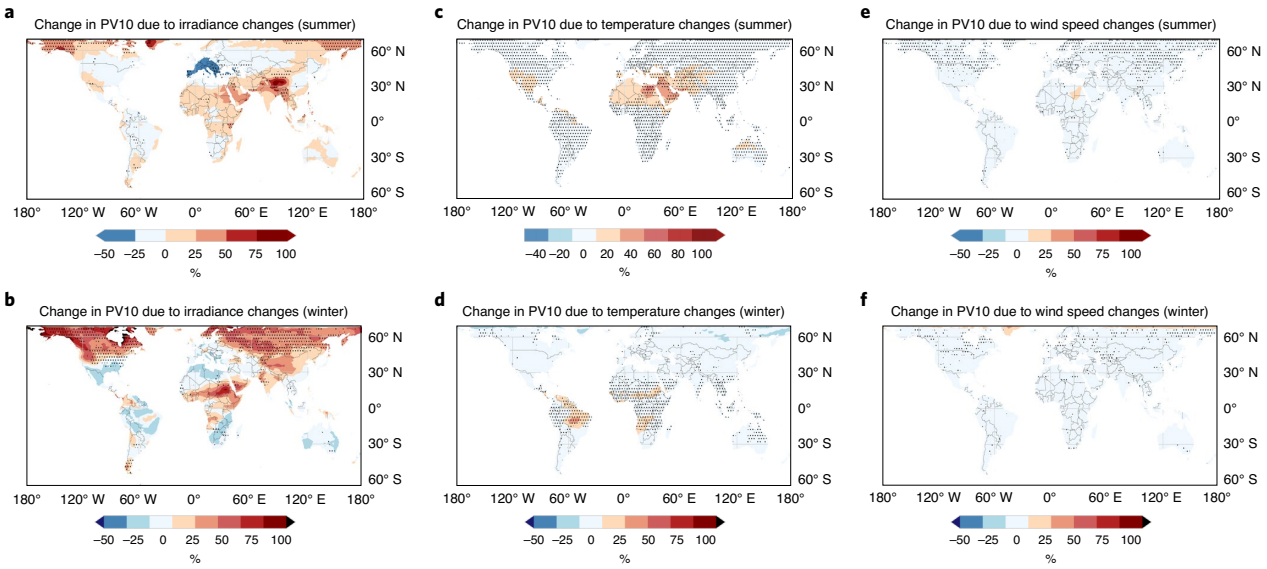

Fig. 4 | Changes in the PV power intermittency are mainly driven by changes in the frequency of cloudy days. Attribution of changes from 1961–1990 to 2036–2065 (RCP4.5) in PV10. **a**–**f**, PV10 changes were computed considering changes in the downwelling SW irradiance only (**a**,**b**), in the surface ambient temperature only (**c**,**d**) and in the surface wind speed only (**e**,**f**). The plots corresponding to summer (**a**,**c**,**e**) were made by assembling DJF data for the Southern Hemisphere and JJA data for the Northern Hemisphere, while the plots corresponding to winter (**b**,**d**,**f**) were made by assembling JJA data for the Southern Hemisphere and DJF data for the Northern Hemisphere. Stippling indicates regions where the detected changes are considered to be significant. The plots were generated using Python's Matplotlib library[43].

that lead to very low PV power outputs is expected to fall. This is the case in southern Europe, where, attributable to a decrease in clouds and aerosols, summer days with very low PV power outputs are expected to drop by half by mid-century, even under a moderate-emission scenario.

The enhanced weather variability associated with the future climate is generally omitted from current estimates of PV power outputs. This omission may compromise the economic sustainability of PV projects. Increases in the number of days with very low PV power outputs may boost PV power intermittency, making it harder to maintain the production/consumption balance within an electrical grid. In particular, substantial increases in the longest event of very low power outputs could affect production costs (because of the need for enhanced energy storage for providing backup power as well as grid stabilization services during these longer events).

Although productivity losses attributable to the enhanced weather variability could probably be overcome by technical improvements[16,33,34] in most regions, our results present useful data for policymakers and energy planners to compensate for the effects of future weather.

Methods

PV_{POT} is defined as the fraction of the power output under standard conditions that a PV module may exhibit in the field[22–26]:

$$PV_{POT} = P_R \frac{I}{I_{STC}}, \quad (1)$$

where I_{STC} is the SW irradiance applied to the module under standard test conditions (1,000 W m^{-2}), I is the SW irradiance impinging on the PV modules in the field and P_R is the so-called performance ratio, which accounts for the effect of the cell temperature (T_{Cell}) on its efficiency. According to prior efforts[23], P_R can be calculated as

$$P_R = 1 - \gamma(T_{Cell} - T_{STC}), \quad (2)$$

where T_{STC} is the cell temperature under standard test conditions (25 °C) and γ can be taken as equal to 0.005 °C^{-1} in the case of monocrystalline silicon cells[39,40].

According to equation (2), a cell temperature higher than 25 °C leads to a poorer performance ratio; T_{Cell} depends on T and v. According to prior efforts[12,23], T_{Cell} can be calculated as

$$T_{Cell} = c_1 + c_2 T + c_3 I - c_4 v, \quad (3)$$

where $c_1 = 4.3$ °C, $c_2 = 0.943$, $c_3 = 0.028$ °C W^{-1} m^2 and $c_4 = 1.528$ °C m^{-1} s. According to equation (3), wind favours cooling of the PV module, leading to a lower cell temperature and in turn to a higher performance ratio.

The actual values of T_{Cell} and P_R may be slightly different from those computed by using equations (2) and (3). These differences will increase (or decrease) the PV_{POT} estimate by a certain proportion; however, since this proportion will affect the PV_{POT} similarly during both the base period and the future period, it has a minor effect on the relative change expected in the PV_{POT}.

Although I, v and T change during the day, following prior efforts[15,23], here we have used daily estimates rendered by GCMs for computing daily estimates of the PV_{POT}. Accordingly, in equation (3), I was taken as equal to daily estimates of the downwelling SW irradiance, v was taken as equal to daily estimates of the surface wind speed and T was taken as equal to daily estimates of the mean surface temperature. In this study, we used daily estimates of I, v and T rendered by seven GCMs from CMIP5 (ref. [27]) (see Supplementary Table 1 for the details). Although tens of CMIP5 models exist, only a fraction of them have daily estimates of the variables of interest. From those with daily data available, we selected models from different providers/institutes (to ensure a fair distribution and representativeness). We checked the coherence and consistency of the GCM-based estimates over the period 1981–2000 by taking the ERA-Interim reanalysis[41] as a reference.

The daily GCM estimates of I, v and T allowed us to compute the daily PV_{POT} values by applying equations (1) through (3). For computing PV_{POT} estimates after 2005, we used GCM simulations according to two scenarios: RCP4.5 and RCP8.5 (ref. [28]).

Following the methodology widely used for assessing changes in the probability of occurrence of extreme events[20,21], we used a 15-day rolling window of the PV_{POT} data over a base period of 30 years (1961–1990) to form datasets of 450 values for each day. The rolling window provides a more robust PDF for the reference period, giving less weight to outliers on a particular day. At each location (or grid point of a climate model), the dataset mean defined a daily base climatology, from which the daily PV_{POT} anomalies could in turn be calculated.

The histogram or the corresponding PDF of the daily PV_{POT} anomalies (the departure of the daily PV_{POT} value from the daily base climatology) allowed us to compute:

PVM: the average of the daily PV_{POT} anomalies. By definition, the PVM estimate is equal to zero over the base period, but, as we have shown in this study,

PVM values computed over a certain period in the future may be notably different due to changes in climate (temperature, wind speed and cloudiness).

SD: the standard deviation of the daily PV_{POT} anomalies. Comparing SD values computed over different periods allowed us in turn to assess changes in the variability of the PV_{POT} anomalies.

PV10: the share of very low daily PV_{POT} values (that is, the fraction of days falling below the 10th percentile of the PV_{POT} anomaly distribution over the base period). The PV10 estimates stand for the share of very low daily PV power outputs, which can be associated with high temperatures or low SW irradiances (caused by clouds and aerosols). By definition, PV10 is equal to 0.10 over the base period, but, as we have shown in this study, PV10 estimates computed over a certain period in the future may be notably different due to changes in the climate (temperature, wind speed and irradiance).

PV10N: the number of events of very low power outputs per season. Each event is a period of at least three consecutive days of very low power outputs (defined according to the 10th percentile).

PV10D: the length in days of the longest event during a season.

PV90: the share of very high daily PV_{POT} values (that is, the fraction of days falling above of the 90th percentile of the PV_{POT} anomaly distribution over the base period). The PV90 estimates stand for the share of very high daily PV power outputs, which can be associated with low temperatures or high SW irradiances (under cloudless and clean conditions). By definition, PV90 is equal to 0.10 over the base period, but, as we have shown in this study, PV90 estimates computed over a certain period in the future may differ considerably.

In this study, the projections for each grid point are based on the MMM of PV10, PV10N, PV10D and PV90 values, computed separately for each GCM. The projections for regions of high solar PV energy potential (the Atacama Desert, southern Europe, the Arabian Peninsula and so on) are based on regional averages computed over the grid points indicated by the red boxes in Supplementary Fig. 10.

As an example, Supplementary Fig. 5 shows the PDFs of the daily summer PV_{POT} anomalies over the base period 1961–1990 (blue PDFs) and the period 2036–2065 (green PDFs for RCP 4.5; red PDFs for RCP8.5) for several regions. Each value used to construct the PDFs in Supplementary Fig. 5 corresponds to a regional average (computed over the grid points within the red boxes shown in Supplementary Fig. 10). The dotted vertical lines in the PDFs in Supplementary Fig. 5 indicate the 10th percentile of the PV_{POT} anomaly distribution corresponding to the base period. Comparing the areas under the PDF curves (from the left to the dotted vertical lines) in Supplementary Fig. 5 allowed us to assess the changes from 1961–1990 to 2036–2065 in summer PV10. The PV10 estimates for each period are indicated in the upper left corner of each panel in Supplementary Fig. 5. These PV estimates allowed us to build up Fig. 3a and Supplementary Fig. 9a. For example, as indicated in the upper left corner of Supplementary Fig. 5b, the PV10 estimates computed from GCM simulations under the RCP4.5 scenario are expected to drop by about 50% (from 0.10 in 1961–1990 to about 0.05 in 2036–2065) in southern Europe.

Changes in both PV10 and PV90 estimates arise from changes in the PDFs shown in Supplementary Fig. 5 (that is, changes in the PVM or the SD of the PDFs). As shown in Supplementary Fig. 5, the regions that exhibit the greatest changes in PV10 and PV90 estimates also exhibit the greatest changes in the SD. For example, under the RCP4.5 scenario, the SD computed from GCM simulations is expected to drop about 6% (from 0.97 in 1961–1990 to 0.91 in 2036–2065) in southern Europe (Supplementary Fig. 5b), while the SD is expected to rise by about 8% by mid-century (from 0.96 and 0.98 in 1961–1990 to 1.03 and 1.06 in 2036–2065) in the Arabian Peninsula (Supplementary Fig. 5c) and in the southwestern United States (Supplementary Fig. 5d), respectively.

Our projections may be affected by the selection of ensembles and models. Although several ensemble members are available for some models, PV_{POT} anomalies were computed by using daily estimates rendered by the first ensemble member of each model. This approach aimed to avoid assigning more weight to one model over the other. Nevertheless, we explored the effect of a different selection by comparing PV10 estimates computed over the period 2036–2065 by using simulations rendered by different ensemble members. We did not find important differences, which suggests that the selection of a specific ensemble member did not substantially affect our outcomes.

We also explored the effects of selecting different models on our results. In particular, we compared changes from 1961–1990 to 2036–2065 in the PV10 estimates computed under the RCP4.5 scenario by using seven GCMs. Supplementary Figs. 11 and 12 show the spread of PV10 changes from different models computed under the RCP4.5 and RCP8.5 scenarios, respectively. Although there are notable intermodel differences in the magnitude of the PV10 changes, the models roughly agree on the direction of the changes. For example, all models show decreases in PV10 estimates in southern Europe by mid-century, while also showing increases in PV10 estimates in the Arabian Peninsula. The intermodel differences were characterized by computing the multimodel standard deviation of decadal PV10 estimates (Supplementary Figs. 11 and 12).

PV10 changes result from changes in wind speed, air temperature and SW irradiance. To disentangle the influence of changes in I, v and T on the PV10 changes, we built up two datasets of the daily PV_{POT} estimates. The first dataset was based on daily PV_{POT} estimates computed by using daily estimates of I, v and T rendered by historical simulations over the period 1961–1990. The second dataset was based on daily PV_{POT} estimates computed by taking projections of a certain variable (I, for example) over the period 2036–2065 (RCP4.5), while taking the same values used in the historical simulations over the period 1961–1990 for the remaining variables. The change in the MMM of the PV10 estimates between these two ensembles allowed us to assess the influence of the changes in I (Fig. 4a,b). To assess the influence of temperature (Fig. 4c,d) and wind speed (Fig. 4e,f), we repeated the same procedure (that is, building up a second dataset by using future projections for the parameter of interest while taking the same values used in the historical simulations for the remaining variables).

The method described above for computing PV10 was also applied for sequentially computing the share of days with very high temperature (T90, according to the 90th percentile), the share of days with very high CF (CF90, according to the 90th percentile) and the share of days with very low surface irradiance (I10, according to the 10th percentile). The thresholds defined by either the 10th or the 90th percentile (of T, CF and I) allowed us, according to the methodology described by Sutanto et al.[38], to create binary maps by assigning each grid cell to 0 if no extreme occurs on a given day or 1 if a very high value of temperature (defined according to the 90th percentile), for example, occurs on that given day. Similar binary maps were created for the days that exhibited very high CFs (also defined according to the 90th percentile) and very low irradiances (defined according to the 10th percentile). These maps enabled us to assess the number of summer days per year with concurrent extremes: very high temperature and heavy clouds (see the first row in Supplementary Fig. 7) or very high temperature, heavy clouds and very low irradiance, simultaneously (see the second row in Supplementary Fig. 7). The maps in Supplementary Fig. 7 (computed for two periods: 1961–1990 and 2036–2065, RCP4.5) confirm that the sharpest drops in the summer PV power outputs expected by mid-century (in northeastern Africa and the Arabian Peninsula) result from the more frequent concurrence of high temperatures and clouds (both above their corresponding 90th percentiles).

Note that the plots corresponding to summer in this Article were made by assembling data computed separately over the period DJF in the Southern Hemisphere and over the period JJA in the Northern Hemisphere. Accordingly, the plots corresponding to winter were made by assembling data computed separately over the period DJF in the Northern Hemisphere and over the period JJA in the Southern Hemisphere. This approach allowed us to better show the effects of unusual weather on the PV_{POT} (which mainly occur in summer for both hemispheres).

Finally, stippling in the plots indicates regions where the detected changes are significant. The adopted significance criteria are based on Field et al.[42]; stippling indicates regions where at least 85% of the models in the cluster (or MMM) agree on the sign of the anomaly and therefore represents features that are robust in the cluster composite. Stippling also indicates regions where the MMM change is greater than one multimodel standard deviation.

Data availability

The data that support the findings of this study are available from the corresponding author upon request. The data from the GCMs were obtained from the World Climate Research Programme's Working Group for CMIP5 (https://esgf-node.llnl.gov/).

Code availability

The code generated during the current study is available from the corresponding author on reasonable request.

Received: 12 April 2020; Accepted: 21 October 2020;
Published online: 16 November 2020

References

1. Feron, S., Cordero, R. R. & Labbe, F. Rural electrification efforts based on off-grid photovoltaic systems in the Andean region: comparative assessment of their sustainability. *Sustainability* **9**, 1825 (2017).
2. *Renewables 2018: Market Analysis and Forecast from 2018 to 2023* (International Energy Agency, 2018); https://www.iea.org/renewables2018/power/
3. Li, X., Mauzerall, D. L. & Bergin, M. H. Global reduction of solar power generation efficiency due to aerosols and panel soiling. *Nat. Sustain.* **3**, 720–727 (2020).
4. Cordero, R. R. et al. Effects of soiling on photovoltaic (PV) modules in the Atacama Desert. *Sci. Rep.* **8**, 13943 (2018).
5. Costa, S. C., Diniz, A. S. A. & Kazmerski, L. L. Dust and soiling issues and impacts relating to solar energy systems: literature review update for 2012–2015. *Renew. Sustain. Energy Rev.* **63**, 33–61 (2016).
6. Lelieveld, J. et al. Global air pollution crossroads over the Mediterranean. *Science* **298**, 794–799 (2002).
7. Gutiérrez, C. et al. Future evolution of surface solar radiation and photovoltaic potential in Europe: investigating the role of aerosols. *Environ. Res. Lett.* **15**, 034035 (2020).

8. Gil, V., Gaertner, M. A., Gutierrez, C. & Losada, T. Impact of climate change on solar irradiation and variability over the Iberian Peninsula using regional climate models. *Int. J. Climatol.* **39**, 1733–1747 (2019).
9. Chen, S. A., Vishwanath, A., Sathe, S. & Kalyanaraman, S. Shedding light on the performance of solar panels: a data-driven view. *SIGKDD Explor.* **17**, 24–36 (2016).
10. Panagea, I. S., Tsanis, I. K., Koutroulis, A. G. & Grillakis, M. G. Climate change impact on photovoltaic energy output: the case of Greece. *Adv. Meteorol.* **2014**, 264506 (2014).
11. Chaichan, M. T. & Kazem, H. A. Experimental analysis of solar intensity on photovoltaic in hot and humid weather conditions. *Int. J. Sci. Eng. Res.* **7**, 91–96 (2016).
12. Chenni, R., Makhlouf, M., Kerbache, T. & Bouzid, A. A detailed modeling method for photovoltaic cells. *Energy* **32**, 1724–1730 (2007).
13. van Ruijven, B. J., De Cian, E. & Sue, I. Wing amplification of future energy demand growth due to climate change. *Nat. Commun.* **10**, 2762 (2019).
14. Wild, M., Folini, D., Henschel, F., Fischer, N. & Müller, B. Projections of long-term changes in solar radiation based on CMIP5 climate models and their influence on energy yields of photovoltaic systems. *Sol. Energy* **116**, 12–24 (2015).
15. Crook, J. A., Jones, L. A., Forster, P. M. & Crook, R. Climate change impacts on future photovoltaic and concentrated solar power energy output. *Energy Environ. Sci.* **4**, 3101–3109 (2011).
16. Gaetani, M. et al. The near future availability of photovoltaic energy in Europe and Africa in climate–aerosol modeling experiments. *Renew. Sustain. Energy Rev.* **38**, 706–716 (2014).
17. Tang, C. et al. Numerical simulation of surface solar radiation over southern Africa. Part 1: evaluation of regional and global climate models. *Clim. Dyn.* **52**, 457–477 (2019).
18. Soares, P. M., Brito, M. C. & Careto, J. A. Persistence of the high solar potential in Africa in a changing climate. *Environ. Res. Lett.* **14**, 124036 (2019).
19. Tang, C. et al. Numerical simulation of surface solar radiation over southern Africa. Part 2: projections of regional and global climate models. *Clim. Dyn.* **53**, 2197–2227 (2019).
20. Feron, S. et al. Observations and projections of heat waves in South America. *Sci. Rep.* **9**, 8173 (2019).
21. Cowan, T. et al. More frequent, longer, and hotter heat waves for Australia in the twenty-first century. *J. Clim.* **27**, 5851–5871 (2014).
22. Bichet, A. et al. Potential impact of climate change on solar resource in Africa for photovoltaic energy: analyses from CORDEX-AFRICA climate experiments. *Environ. Res. Lett.* **14**, 124039 (2019).
23. Jerez, S. et al. The impact of climate change on photovoltaic power generation in Europe. *Nat. Commun.* **6**, 10014 (2015).
24. Jerez, S. et al. Future changes, or lack thereof, in the temporal variability of the combined wind-plus-solar power production in Europe. *Renew. Energy* **139**, 251–260 (2019).
25. Ravestein, P., Van der Schrier, G., Haarsma, R., Scheele, R. & Van den Broek, M. Vulnerability of European intermittent renewable energy supply to climate change and climate variability. *Renew. Sustain. Energy Rev.* **97**, 497–508 (2018).
26. Mavromatakis, F. et al. Modeling the photovoltaic potential of a site. *Renew. Energy* **35**, 1387–1390 (2010).
27. Taylor, K. E., Stouffer, R. J. & Meehl, G. A. An overview of CMIP5 and the experiment design. *Bull. Am. Meteorol.* **93**, 485–498 (2012).
28. Thomson, A. M. et al. RCP4.5: a pathway for stabilization of radiative forcing by 2100. *Clim. Change* **109**, 77–94 (2011).
29. Huld, T. et al. in *The Availability of Renewable Energies in a Changing Africa* Report No. EUR 25980 EN (European Commission, 2013); https://doi.org/10.2790/88194
30. Boé, J., Somot, S., Corre, L. & Nabat, P. Large discrepancies in summer climate change over Europe as projected by global and regional climate models: causes and consequences. *Clim. Dyn.* **54**, 2981–3002 (2020).
31. Biasutti, M. Forced Sahel rainfall trends in the CMIP5 archive. *Geophys. Res. Atmos.* **118**, 1613–1623 (2013).
32. Vihma, T. et al. The atmospheric role in the Arctic water cycle: a review on processes, past and future changes, and their impacts. *J. Geophys. Res.* **121**, 586–620 (2016).
33. Abujarad, S. Y., Mustafa, M. W. & Jamian, J. J. Recent approaches of unit commitment in the presence of intermittent renewable energy resources: a review. *Renew. Sustain. Energy Rev.* **70**, 215–223 (2017).
34. Kittner, N., Lill, F. & Kammen, D. M. Energy storage deployment and innovation for the clean energy transition. *Nat. Energy* **2**, 17125 (2017).
35. Ruosteenoja, K., Räisänen, P., Devraj, S., Garud, S. S. & Lindfors, A. V. Future changes in incident surface solar radiation and contributing factors in India in CMIP5 climate model simulations. *J. Appl. Meteorol. Clim.* **58**, 19–35 (2019).
36. Merlone, A. et al. Temperature extreme records: World Meteorological Organization metrological and meteorological evaluation of the 54.0 °C observations in Mitribah, Kuwait and Turbat, Pakistan in 2016/2017. *Int. J. Climatol.* **39**, 5154–5169 (2019).
37. Lelieveld, J. et al. Strongly increasing heat extremes in the Middle East and North Africa (MENA) in the 21st century. *Clim. Change* **137**, 245–260 (2016).
38. Sutanto, S. J., Vitolo, C., Di Napoli, C., D'Andrea, M. & Van Lanen, H. A. Heatwaves, droughts, and fires: exploring compound and cascading dry hazards at the pan-European scale. *Environ. Int.* **134**, 105276 (2020).
39. Tonui, J. K. & Tripanagnostopoulos, Y. Performance improvement of PV/T solar collectors with natural air flow operation. *Sol. Energy* **82**, 1–12 (2008).
40. Pérez, J. C., González, A., Díaz, J. P., Expósito, F. J. & Felipe, J. Climate change impact on future photovoltaic resource potential in an orographically complex archipelago, the Canary Islands. *Renew. Energy* **133**, 749–759 (2019).
41. Dee, D. P. et al. ERA-Interim reanalysis: configuration and performance of the data assimilation system. *Q. J. R. Meteorol. Soc.* **137**, 553–597 (2011).
42. Field, C. B., Barros, V., Stocker, T. F. & Dahe, Q. (eds) *Managing the Risks of Extreme Events and Disasters to Advance Climate Change Adaptation: Special Report of the Intergovernmental Panel on Climate Change* (Cambridge Univ. Press, 2012).
43. Hunter, J. D. Matplotlib: a 2D graphics environment. *Comput. Sci. Eng.* **9**, 90–95 (2007).

Acknowledgements

We acknowledge the support of FONDECYT (Preis 1191932) and CORFO (Preis 19BP-117358, 18BPCR-89100 and 18BPE-93920). A.D. was supported by the JST CREST grant number JPMJCR15K4. We also thank the World Climate Research Programme's Working Group on Coupled Modelling, which is responsible for CMIP, and we thank the climate modelling groups used in this study for producing and making available their model outputs.

Author contributions

S.F., R.R.C. and R.B.J. conceived and designed the experiments. S.F., R.R.C. and A.D. analysed the data. S.F., R.R.C. and R.B.J. wrote the paper.

Competing interests

The authors declare no competing interests.

Additional information

Supplementary information is available for this paper at https://doi.org/10.1038/s41893-020-00643-w.

Correspondence and requests for materials should be addressed to R.R.C.

Peer review information *Nature Sustainability* thanks Jose Bilbao and the other, anonymous, reviewer(s) for their contribution to the peer review of this work.

Reprints and permissions information is available at www.nature.com/reprints.

Publisher's note Springer Nature remains neutral with regard to jurisdictional claims in published maps and institutional affiliations.